JOURNAL OF MATERIALS SCIENCE **33** (1998) 5695–5702

Fabrication of β- and β''-Al_2O_3 tubes by pressureless powder packing forming and salt infiltration

JEONG-HYUN PARK*, KYUNG-HEE KIM*, JEONG-MAN CHO*, SUNG-KI LIM**
*Department of Ceramic Engineering, Yonsei University, Seoul, 120-749, Korea, **Department of Industrial Chemistry, Konkuk University, Seoul, 133-701, Korea
E-mail: citylite@kriss.re.kr

A new forming method, pressureless powder packing (PLPP), was studied to fabricate the β- and β''-Al_2O_3 tubes. Alkali sources were infiltrated into the pores of α-Al_2O_3 tube preforms that had been prepared by the PLPP forming method. The composition for the synthesis of β''-Al_2O_3 phase was $Na_2O \cdot 0.138Li_2O \cdot 4.4Al_2O_3$. The β''-Al_2O_3 fraction of calcined and sintered bodies was increased with the increase of calcination temperature, and phase formation was largely affected by the type of starting α-Al_2O_3. Large particle size and narrow size distribution of fused α-Al_2O_3 resulted in uniform green microstructure that enhanced the homogeneity of alkali salts after infiltration, which was very important for the β''-Al_2O_3 formation. Sintered microstructure was uniform in all specimens but further development was required for density improvement.

1. Introduction

β- and β''-Al_2O_3 have been developed because of their highly ionic and low electronic conductivity, and research for their practical use has been widely performed. Na^+ ions act as charge carriers in β- and β''-Al_2O_3, which have been used as solid electrolytes in a Na/S secondary battery for electric vehicles and storage of excess electricity [1–3].

Usually β- and β''-Al_2O_3 are prepared by conventional ceramic processing. First, raw materials are prepared by various process, such as spray drying, freeze drying, sol-gel method, coprecipitation, and mechanical mixing [4–7]. After calcination, synthesized β- and β''-Al_2O_3 powders are formed to tubes by (cold isostatic pressing CIP), slip casting, and electrophoretic deposition and then are sintered [8–10].

PLPP forming is a new fabrication method. Preform is made by packing powder in the rubber mold with vibration, and then binder solution is infiltrated to consolidate the packed powders. Removing the mold after drying completes the forming process. The merits of PLPP forming are the ease of forming complex shapes with powders that have large particle size and irregular particle shape and no stress gradient in the green body [11].

In conventional ceramic processing to prepare β- and β''-Al_2O_3, the starting α-Al_2O_3 powder has to be fine and very reactive to obtain good properties during densification and phase formation, and tubes usually have to be made of the partly or fully synthesized β- and β''-Al_2O_3 powders. In the PLPP method, β- and β''-Al_2O_3 can be prepared from the powder that has large particle size and unreactive surface, and tubes are made of α-Al_2O_3 powder before β- and β''-Al_2O_3 phase synthesis.

The purpose of the present study is to fabricate the β- and β''-Al_2O_3 tubes using α-Al_2O_3 preforms fabricated by the PLPP forming method. Different α-Al_2O_3 powders, such as fused α-Al_2O_3, calcined α-Al_2O_3, and mixtures of fused and calcined α-Al_2O_3 were used to prepare preforms, and the green microstructures were compared with each other. The influences of the composition and particle size of the starting α-Al_2O_3 powders and calcination temperatures on β- and β''-phase formation, densification, and microstructure were examined.

2. Experimental

2.1. Preparation of β''-Al_2O_3 preform

α-Al_2O_3 ($\geq$ 99% and reagent-grade salts were used as starting materials. Figs. 1 and 2 show the characteristics of the starting α-Al_2O_3. All powders had narrow particle size distributions. Fused α-Al_2O_3, was coarse powder with angular shapes and had average particle sizes of 19 μm and 33 μm. Calcined α-Al_2O_3 was fine powder with spherical shape and had an average particle size of 0.4 μm.

Five kinds of preforms were prepared. Preforms of fused α-Al_2O_3 were classified as W1 (33 μm) and W2 (19 μm). Preforms of calcined α-Al_2O_3 were classified as AKP-30. Fused α-Al_2O_3 of W1 and W2 as mixed with calcined α-Al_2O_3 by the weight ratio of 2 : 1 and designated as W1A and W2A, respectively. Fused and calcined α-Al_2O_3 powders were dry mixed by low speed stirrer without liquid medium to avoid agglomeration. The whole forming procedure of PLPP method is shown in Fig. 3. The α-Al_2O_3 powders were

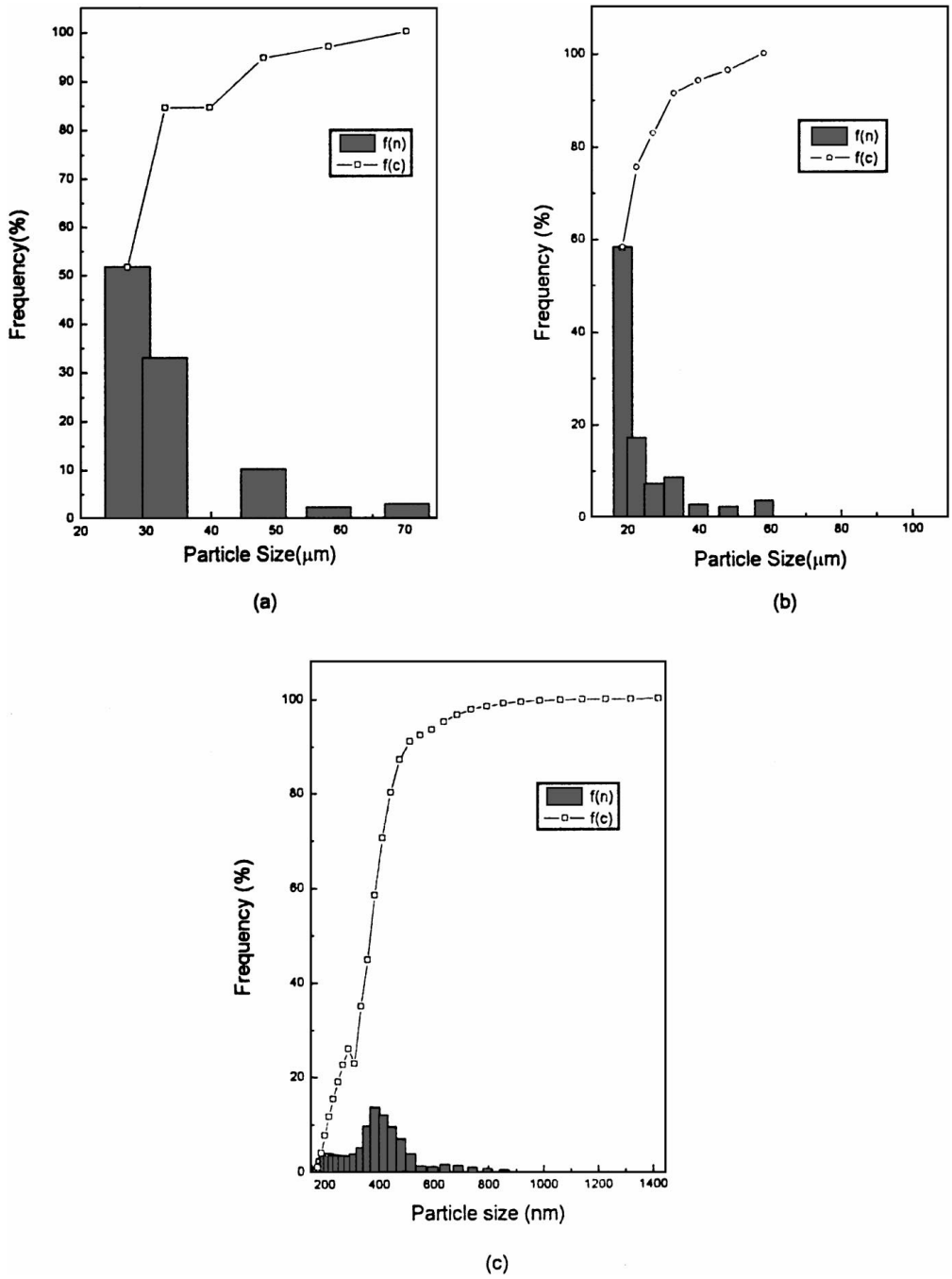

Figure 1 Particle size analyses of starting powders (a) W1, (b) W2, (c) AKP-30.

poured into the silicon rubber mold and then packed by mechanical vibration using a vibrator for which output and maximum frequency were 50 W and 83 Hz, respectively.

The binder solution was made by dissolving 2 wt % PVA (polyvinyl alcohol) in water and was infiltrated into the packed powder within the mold. For calcined α-Al_2O_3, binder solution seemed to cause the particle agglomeration and nonuniform internal structure, thus, after infiltration, the mold packed with calcined α-Al_2O_3 was vibrated again to minimize the agglomeration. After infiltration, preforms were dried at 70 °C in an oven and taken out of the mold. Preform tubes were 1.5 mm thick, 24.6 mm in diameter, and 120 mm in length. Formed bodies of calcined α-Al_2O_3, fused α-Al_2O_3, and mixtures were heated at 1100 °C for 2 h, 1700 °C for 2 h, and 1400 °C for 2 h, respectively, to burn out binder and give strength for handling. The photograph of preforms after heat treatment is shown in Fig. 4.

Particle shape and particle size distribution of α-Al_2O_3 powders were observed by the particle size analyzer and scanning electron microscope (SEM). Packing density was measured by following ASTM D4512. Green density of the preform was measured by Archimedes method and pore size distribution and average pore size were investigated by mercury porosimetry.

2.2. Infiltration and calcination

Composition for β- and β''-Al_2O_3 was Li_2O 0.8 wt %, Na_2O 12 wt %, and Al_2O_3 87.2 wt %, which included

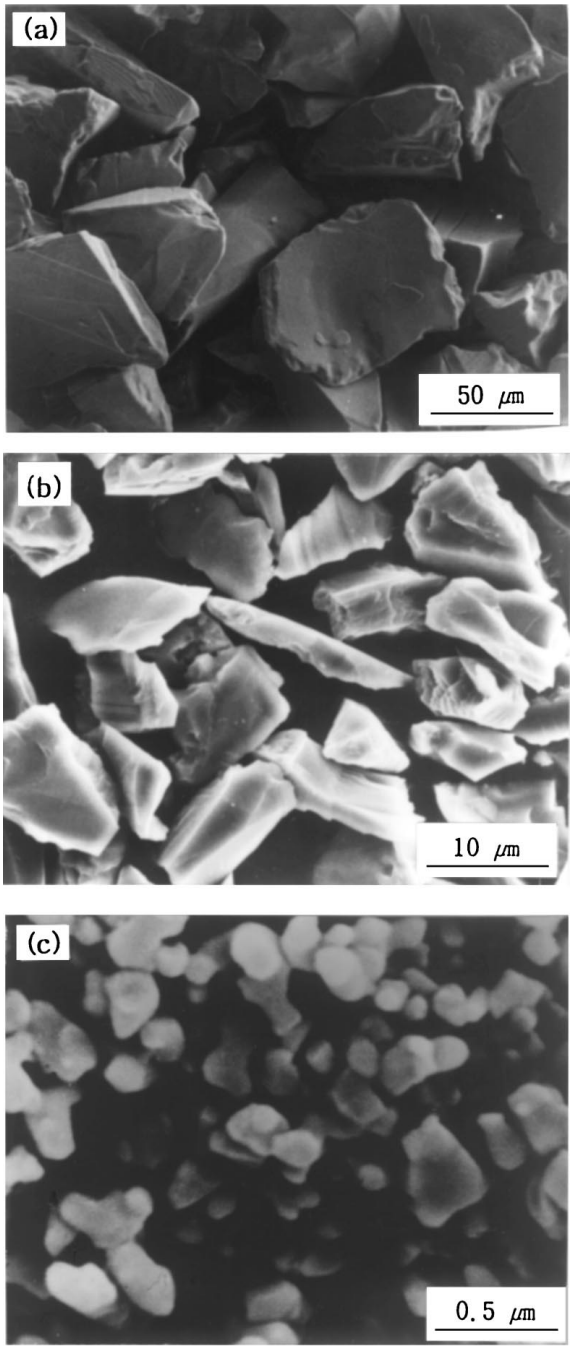

Figure 2 SEM micrographs of starting powders (a) W1, (b) W2, (c) AKP-30.

the excess amount Na_2O by 2 wt % for compensating the Na loss that should occur at high temperature.

$NaNO_3$ and $LiNO_3$ were used as Na and Li sources. The eutectic temperature of $NaNO_3$ and $LiNO_3$ is 191 °C at eutectic composition but was raised to ≈280 °C for the composition of this experiment. Li and Na salts were mixed and melted completely at the range of 300–350 °C and then infiltrated into the preform by capillary force. After infiltration, preforms were weighed and excess salts were washed by dipping the preforms in boiling water for a few seconds. When the preforms were of insufficient weight, molten salts were reinfiltrated to obtain the exact composition. The infiltrated bodies were calcined at 1350–1550 °C for 4 h with the heating rate of 300 °C/h.

2.3. Sintering

Sintering was carried out by a two-peak firing schedule [12]. MgO crucibles and a powder bed of same composition with tubes were used to minimize the Na loss. Average heating rate was 360 °C/h. First peak was at 1550 °C for 5 min and then cooled to 1400 °C, and second peak was at 1650 °C for 15 min.

Phase analysis was done by X-ray powder diffraction. The microstructures were compared by examination of the fractured surfaces of specimens. Bulk densities of sintered specimens were measured by Archimedes method using kerosene, with a specific gravity of 0.81, following the ASTM C830. The theoretical densities of specimens were calculated by mixing rule, considering the relative ratios of each phase, where the theoretical densities of β- and β''-Al_2O_3 are 3.24 /cm^3 and 3.27 g/cm^3, respectively.

3. Results and discussion

3.1. Properties of preforms

Generally, packing density is a function of time, mechanical vibration frequency, and size of the starting powder. Small particle size causes difficulty in attaining a high packing density. If particle size is smaller than 100 μm, friction and bridging between particles can easily happen, and the increase of surface energy by increased relative surface area causes the particle agglomeration by moisture adsorption and particle cohesion. The decrease of particle size means the decrese of each particle mass and the influence of gravity, thus packing density lowers [13].

Table I summarizes the properties of the starting powders and preforms. The packing density is higher in the order of W1, W1A, W2, W2A, and AKP-30. W1 and W1A showed a slightly higher packing density because of their relatively large particle size and low agglomeration effect between powders. W1A and W2A are expected to have higher packing density than W1 and W2 have because powders with broad particle size distribution and mixture of powders of different particle sizes should have higher packing density than monosized and unmixed ones [13]. Packing densities of W1A and W2A, however, showed slightly lower value than those of W1 and W2, respectively, which seemed to be attributed to the agglomerations of calcined α-Al_2O_3. W1A had slightly higher packing density than W2A had because of the same agglomeration effect due to the particle size difference.

In previous experiments, if green density was higher than 70% of theoretical density, salts infiltration and β- and β''-Al_2O_3 formation were insufficient. In addition, unreacted α-Al_2O_3 phase still remained after calcination and sintering. It was intended that green densities of preforms had the value near 50% of theoretical density and actually were 51–57%, as presented in Table I. Low packing density of calcined α-Al_2O_3 could be overcome by mechanical vibration after infiltrating binder solution. Liquid phase can cause compressive stress between particles [14]. Compressive stress caused by PVA solution and mechanical vibration seemed to rupture

TABLE I Properties of powders and preforms

Designation	Packing density of powders (%)	Heat treatment	Green density of preforms (%)	Linear shrinkage of preforms (%)
W1	49.3	1700 °C, 2 h	51	7.9
W2	47.8	1700 °C, 2 h	53	6.86
W1A	48.3	1400 °C, 2 h	52	5.65
W2A	47.2	1400 °C, 2 h	53	3.75
AKP-30	39.0	1100 °C, 2 h	57	3.5

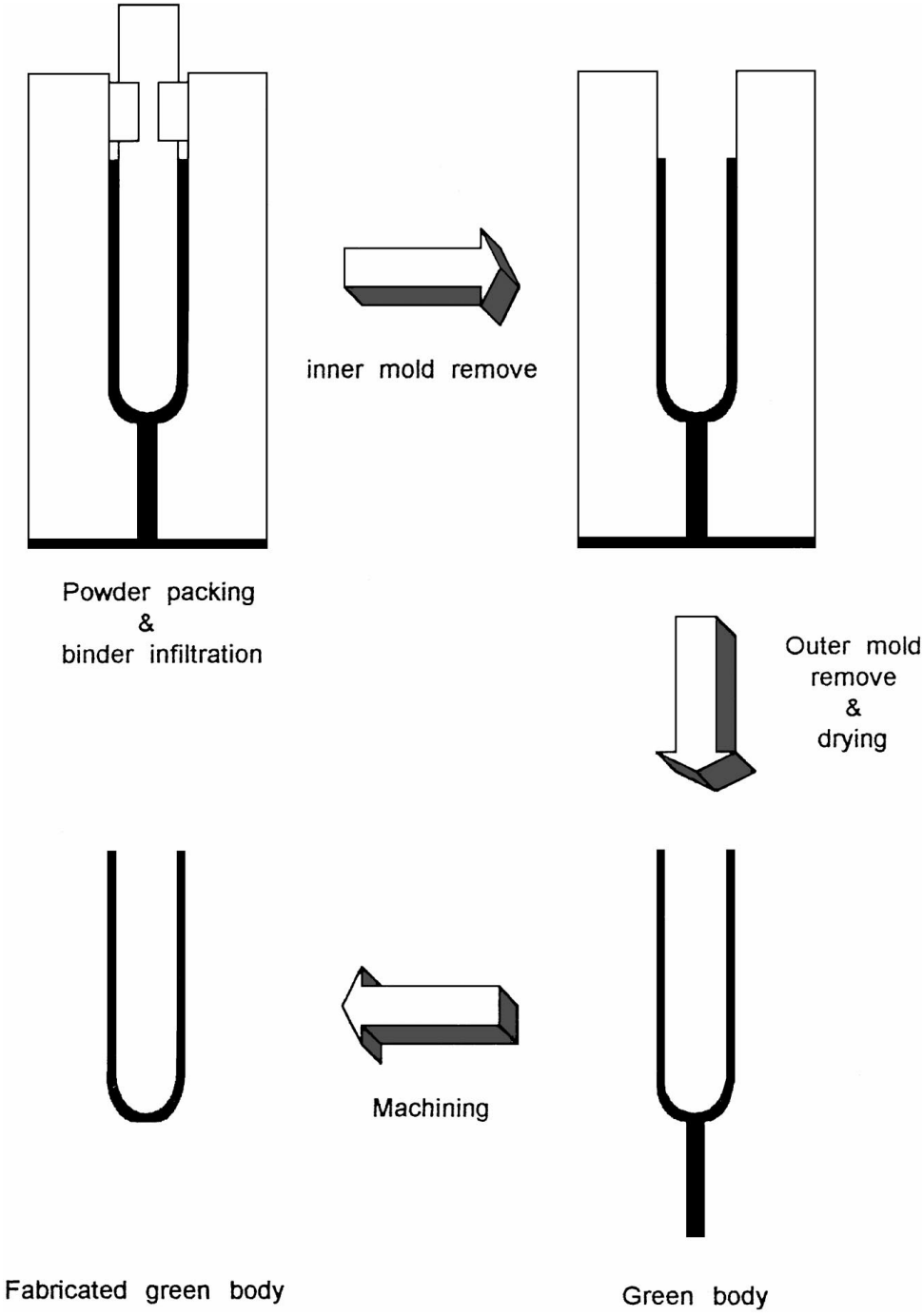

Figure 3 Schematic representation of overall tube forming process by PLPP forming method.

some part of agglomeration and make particles rearrange through rolling and sliding.

Fig. 5 represents the pore size distributions of preforms, which had a significant influence on the infiltration of salts. Preforms of W1 and W2 had unimodal and narrow pore size distributions and had average pore sizes of 13 μm and 8.7 μm, respectively, without pores less than 1 μm. Preforms of W1A and W2A had trimodal pore size distributions, and most pores were in the range of 2–13 μm and 1–11 μm, respectively. These nonuniform pore size distributions are attributed to the heterogeneous regions that occurred during mixing, agglomeration of calcined α-Al_2O_3, and shrinkage differences between calcined and fused α-Al_2O_3 during heat

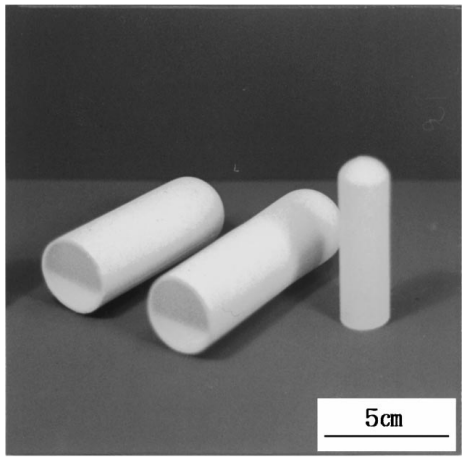

Figure 4 Photograph of fabricated one-ended α-Al_2O_3 tube preforms.

treatment. AKP-30 had bimodal pore size distribution, and two peaks existed at 10.6 μm and 1 μm.

3.2. Properties of sintered tubes

3.2.1. Phase analysis

β- to β''-Al_2O_3 transformation mechanisms have not been fully resolved to date, but Hodge [15] proposed the reaction as follows:

$$\beta\text{-}Al_2O_3 + \delta\text{-}NaAlO_2 = \beta''\text{-}Al_2O_3$$

δ-$NaAlO_2$ is an unstable phase and exists only at the high temperature range and as γ-$NaAlO_2$ in the room temperature range. δ-$NaAlO_2$ exists at grain boundaries and reacts with β-Al_2O_3 to form β''-Al_2O_3 [16]. Without stabilizer or with excess Na_2O, δ-$NaAlO_2$ separates into unreacted γ-$NaAlO_2$ and β-Al_2O_3 [15]. Unreacted γ-$NaAlO_2$ exists at low temperature and is dependent on the Na_2O content, which begins to appear when Na_2O content is over 10.5 wt % [17].

β- and β''-Al_2O_3 have similar structural forms and are non-stoichiometric compounds. β- and β''-Al_2O_3 phases can be identified by X-ray powder diffraction method [18], and the quantitative amount of each phase can be calculated by the following formula comparing the characteristic peaks of each phase [19]:

$$f(\beta'') = 1.37I(\beta'', d = 2.609)/\{I(\beta, d = 2.69) + 1.37I(\beta'', d = 2.609)\}$$

Fig. 6 represents the β''-Al_2O_3 fractions of calcined specimens as a function of calcination temperature. After calcination, the β''-Al_2O_3 fraction was higher in fused α-Al_2O_3 of W1 and W2 and had the range of 50–70%. In mixtures (W1A and W2A), β''-Al_2O_3 had reduced value of 40–60%, and calcined α-Al_2O_3 had the lowest β''-Al_2O_3 fraction of 30–50%. The β''-Al_2O_3 fraction slightly increased with increasing calcination temperature and was maintained at higher temperatures over 1450 °C.

Fig. 7 shows the β''-Al_2O_3 fractions of sintered specimens as a function of calcination temperature. After sintering, the β''-Al_2O_3 phase was well-synthesized in the specimens of W1 and W2, which had fractions of

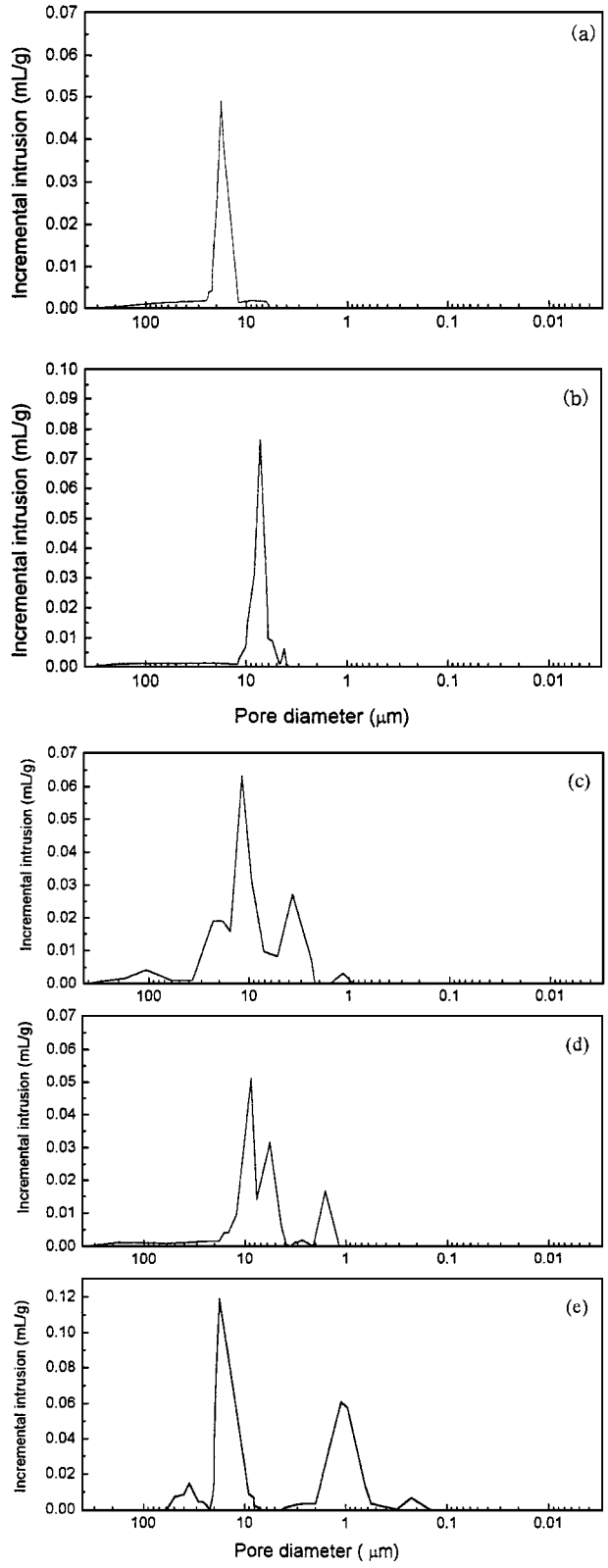

Figure 5 Pore size distributions of α-Al_2O_3 preforms (a) W1, (b) W2, (c) W1A, (d) W2A, (e) AKP-30.

89–93% and 88–92%, respectively. W1A and W2A showed lower β''-Al_2O_3 fractions than W1 and W2 had and were 82–87% and 81–86%, respectively. In the AKP-30, β''-Al_2O_3 was in the range of 78–85%.

It was considered that green microstructures of the preforms had a significant influence on the β''-Al_2O_3 synthesis. Uniform pore structure and large pore channels in the preform resulted in the uniform distribution of alkali salts that were the sources for β''-Al_2O_3 phase

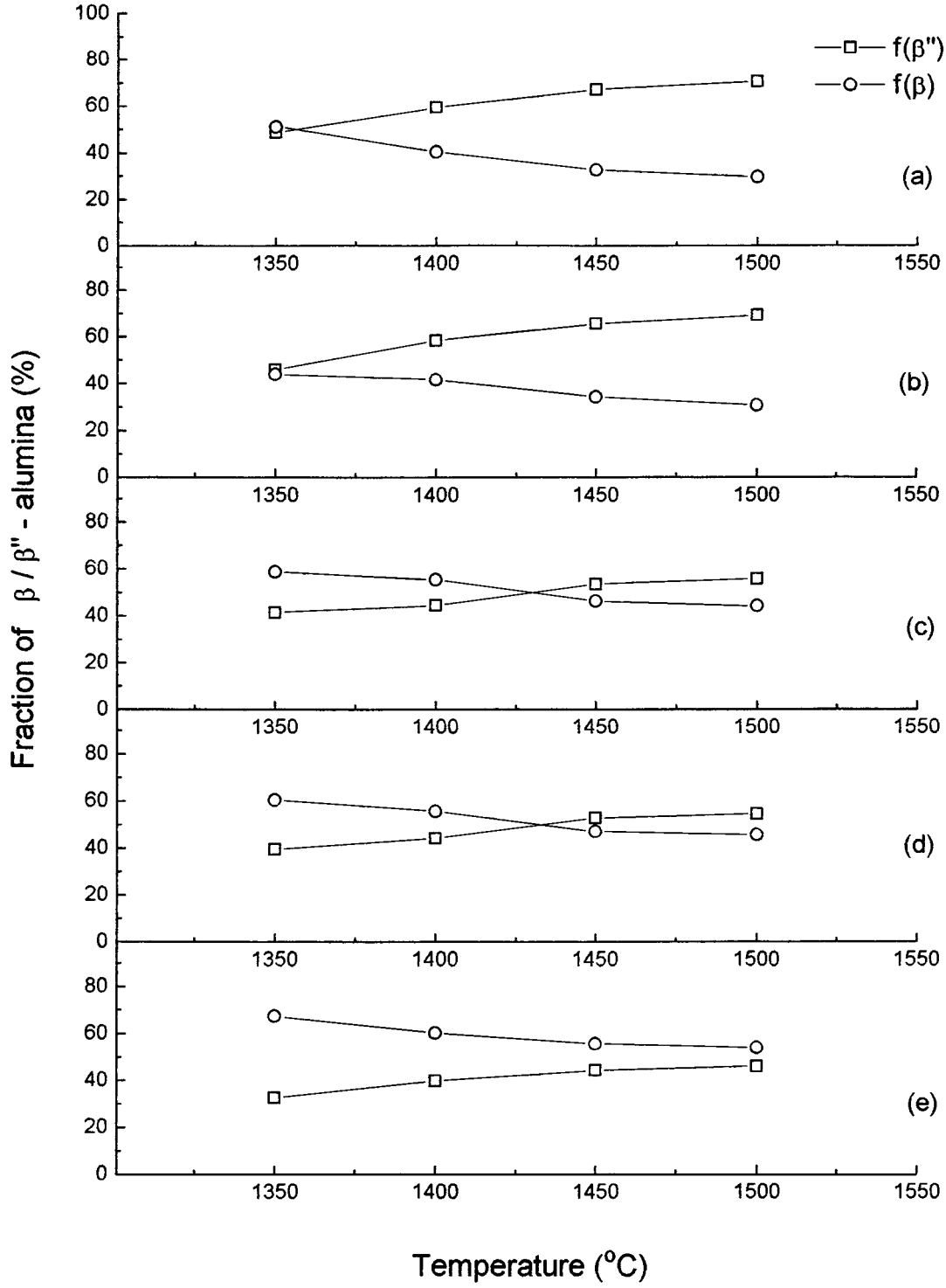

Figure 6 β- and β''-Al_2O_3 fraction of calcined specimens (a) W1, (b) W2, (c) W1A, (d) W2A, (e) AKP-30.

formation. Preforms of fused α-Al_2O_3 had uniform pore structures and high packing densities that enabled uniform distribution of molten salts during infiltration and less local inhomogeneity in preforms. Therefore, specimens started from fused α-Al_2O_3 showed better β''-phase synthesis characteristics than did those from mixed powders and calcined α-Al_2O_3.

3.2.2. Sintering behaviour

The main problems during β- and β''-Al_2O_3 sintering are the evaporation of Na and the appearance of duplex microstructure. Na evaporation makes β''-Al_2O_3 decompose and is the direct cause of the degradation of electrical properties by decreasing the number of charge carriers, the Na^+ ions. Duplex microstructures, especially the exaggerated grain growth, are found to degrade the mechanical properties and have to be avoided [1, 20]. Thus, sintering should take a short time to prevent Na loss and exaggerated grain growth.

It is typical for β- and β''-Al_2O_3 to show a fast densification rate, whereas the transformation rate from β- to β''-Al_2O_3 is slow [15, 21]. Therefore, long duration at sintering temperature for phase tranformation will cause the severe loss of Na. To keep the Na^+ ions in the structure, specimens should be embedded in powders

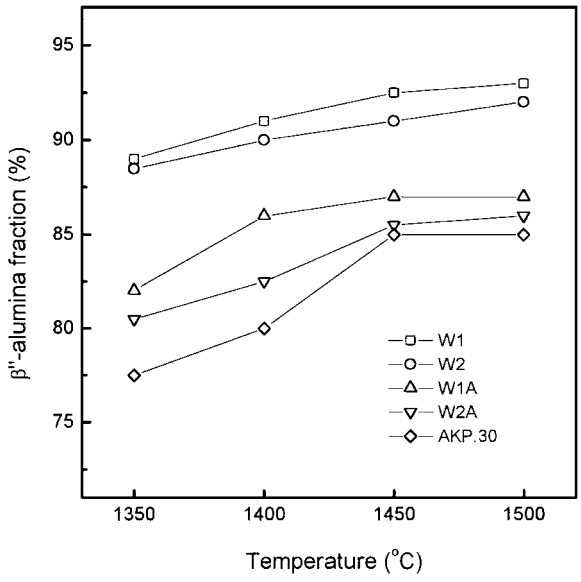

Figure 7 β''-Al_2O_3 fraction of sintered specimens as a function of calcination temperature.

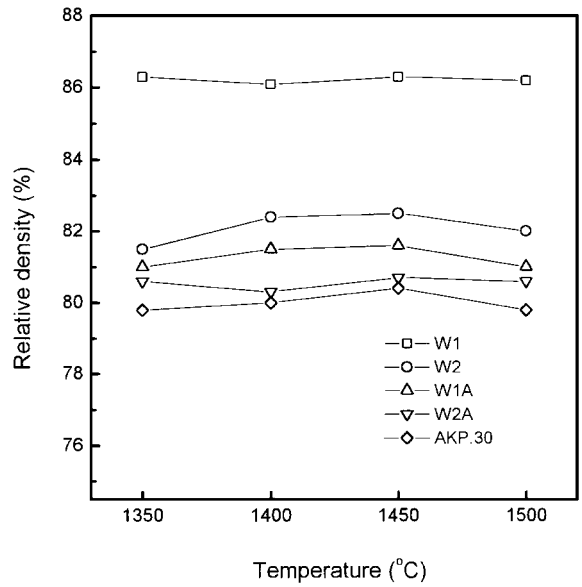

Figure 8 Relative density of sintered specimens as a function of calcination temperature.

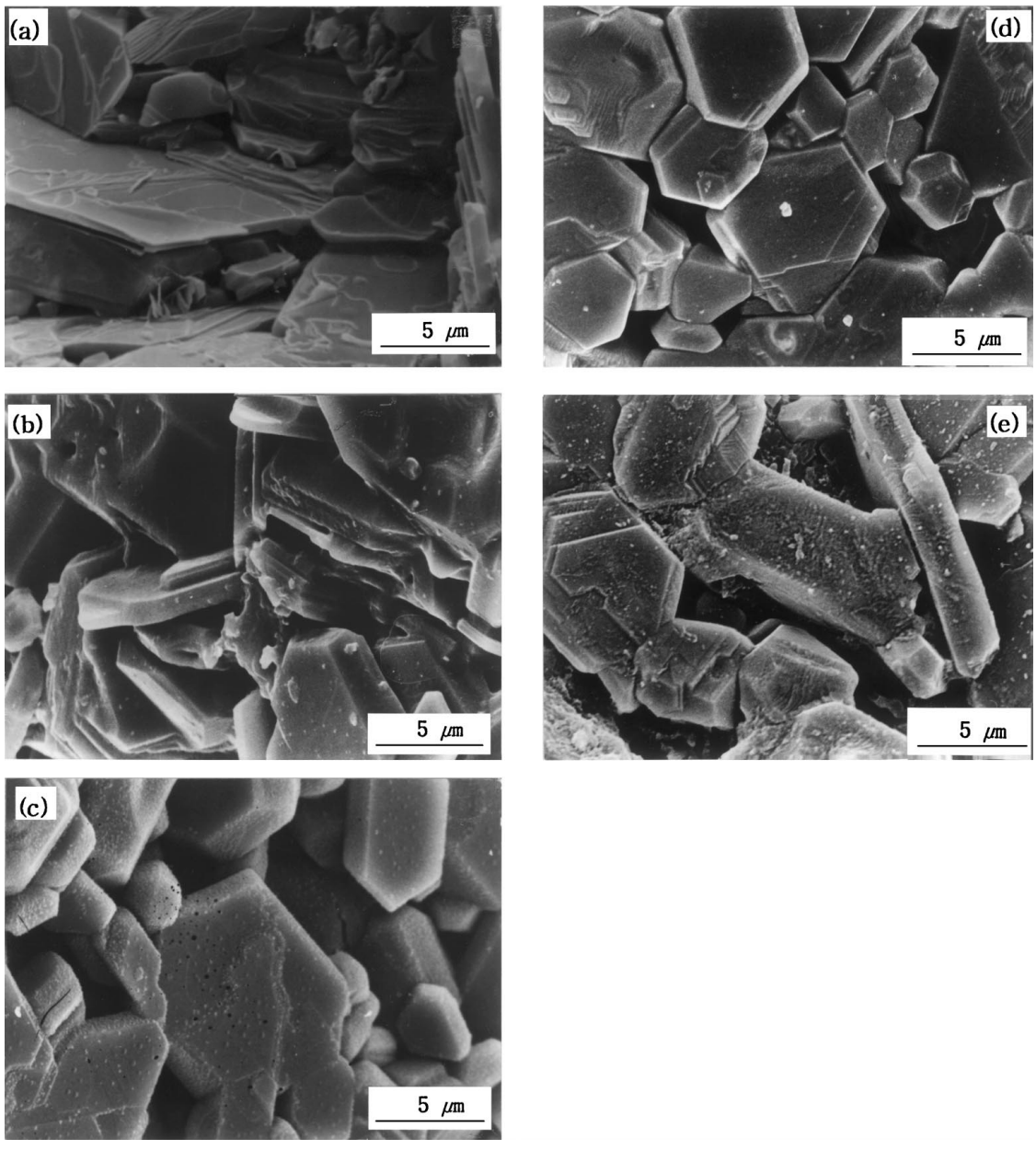

Figure 9 SEM micrographs of fracture surfaces of sintered specimens (a) W1, (b) W2, (c) W1A, (d) W2A, (e) AKP-30.

of same composition and sintered in MgO crucibles to suppress Na evaporation [1].

Some sintering schedules to enhance the properties of β- and β''-Al_2O_3 have been reported, including post-sintering annealing [7] and zone sintering [22, 23]. These sintering processes were effective at preventing the Na loss but were accompanied by the duplex structures that had both fine grains and platelike exaggerated grains with sizes over 100 μm.

To prevent the duplex microstructures, Duncan and Bugden [12] suggested the two-peak firing schedule that included two peaks of temperature during firing; one was 1500–1575 °C and the other was 1600–1650 °C. Specimens are heated up to the first peak and cooled down by 170–200 °C and then heated up to the second peak and held for 5–15 min. By using this two-peak firing schedule, the average grain size increased, but exaggerated grain growth could be hindered, and uniform microstructure could be obtained.

In this experiment, sintering was carried out by the two-peak firing schedule. Fig. 8 represents the relative sintered density. The changes of density as a function of calcination temperature are little. The relative density of W1 showed the highest value of 86%. Relative densities of W1A and AKP-30 were 81% and 80%, respectively. In order to enhance the densification, fused α-Al_2O_3 was mixed with calcined α-Al_2O_3 for the purpose of filling the voids of fused α-Al_2O_3 particles with calcined α-Al_2O_3. Sintered densities of mixed powders, however, were not as high as expected. As discussed previously, it is thought that the low density of W1A and AKP-30 was due to the agglomeration of calcined α-Al_2O_3 that was not destroyed by mechanical vibration and to the shrinkage difference between fused and calcined α-Al_2O_3 that gave rise to local inhomogeneity and large pores.

Fused α-Al_2O_3 is not easy to densify due to its manufacturing process. Therefore, to obtain high density, it demands more investigation, such as raising sintering temperature and filling the voids with larger amounts of alkali salts.

Microstructures of sintered specimens that had calcined at 1450 °C for 4 h are shown in Fig. 9. All specimens showed platelike grains. In the case of W1, uniform microstructure with grain size range of 20–30 μm was observed. Considering the average particle size of starting powder, it could be assured that abnormal grain growth did not occur. In W2, grains with the size of 10–20 μm were observed. A sintered specimen started from calcined α-Al_2O_3 had grains smaller than 20 μm. W1A and W2A of mixed powders had large grains and small grains smaller than 5 μm that originated from calcined α-Al_2O_3.

4. Conclusion

α-Al_2O_3 preforms with relative densities of 51–57% prepared by PLPP method were used to fabricate β- and β''-Al_2O_3 tubes. To synthesize the β- and β''-Al_2O_3 phase, molten salts of $NaNO_3$ and $LiNO_3$ with the compositions of $Na_2O \cdot 0.138Li_2O \cdot 4.4Al_2O_3$ were infiltrated as alkali sources. Phase transformation and densification were highly dependent on the type of starting α-Al_2O_3 powders and the calcination temperature. For fused α-Al_2O_3 with average particle sizes of 19 μm and 33 μm, the β''-Al_2O_3 tube was well-synthesized and had high fractions of 92% and 93%, respectively. It seemed to be caused by uniform green microstructures of fused α-Al_2O_3 that resulted in the homogeneous infiltration of salts. After calcination and sintering, the β''-Al_2O_3 phase increased with the increase of calcination temperature in all specimens. Uniform microstructure of platelike grains could be obtained by adopting two-peak firing schedule for sintering.

References

1. J. T. KUMMER and N. WEBER, *Soc. Automot. Eng. Trans.* **76** (1968) 1003.
2. J. L. SUDWORTH and A. R. TILLEY, "The Sodium Sulfur Battery" (Chapman & Hall, London, 1985).
3. J. E. BATTLES, *Intern. Mater. Rev.* **34** (1989) 1.
4. D. W. JOHNSON JR., S. M. GRANSTAFF, JR. and W. W. RHODES, *Amer. Ceram. Soc. Bull.* **58** (1979) 849.
5. J. D. HODGE, *Amer. Ceram. Soc. Bull.* **62** (1983) 244.
6. J. H. CHOY, J. S. YOO, Y. S. HAN and Y. H. KIM, *Mater. Lett.* **16** (1993) 226.
7. G. YOUNGBLOOD, A. V. VIRCAR, W. R. CANNON and R. S. GORDON, *Amer. Ceram. Soc. Bull.* **56** (1977) 206.
8. M. L. MILLER, B. J. MCENTIRE, G. E. MILLER and R. S. GORDON, *Amer. Ceram. Soc. Bull.* **58** (1979) 522.
9. M. RIVIER and A. D. PELTON, *Amer. Ceram. Soc. Bull.* **57** (1978) 183.
10. R. W. POWERS, *Amer. Ceram. Soc. Bull.* **65** (1986) 1270.
11. J. H. PARK and J. S. SUNG, *J. Korean Ceram. Soc.* **32** (1995) 113.
12. J. H. DUNCAN and W. G. BUGDEN, *Proc. Brit. Ceram. Soc.* **31** (1981) p. 221.
13. R. M. GERMAN, "Particle Packing Characteristics" (Metal Powder Industries Federation).
14. J. S. REED, "Introduction to the Principles of Ceramic Processing" (John Wiley & Sons, New York, 1988).
15. J. D. HODGE, *J. Amer. Ceram. Soc.* **66** (1983) 166.
16. Y. HIRATA, *J. Mater. Res.* **6** (1991) 585.
17. H. I. SONG, E. S. KIM and K. H. YOON, *Physica* **B150** (1988) 148.
18. C. SHMID, *J. Mater. Sci. Lett.* **5** (1986) 263.
19. K. KURIBAYASHI and P. S. NICHOLSON, *Mater. Res. Bull.* **15** (1980) 1595.
20. A. V. VIRKAR and R. S. GORDON, in "Ceramic Microstructure '76: with emphasis on energy related applications," edited by R. M. Fulrath and J. A. Park (Westview Press, Boulder, CO, 1976) p. 610.
21. R. C. DE VRIES and W. L. ROTH, *J. Amer. Ceram. Soc.* **52** (1969) 364.
22. I. W. JONES and L. J. MILES, *Proc. Brit. Ceram. Soc.* **19** (1971) 161.
23. M. Y. HSIESH and L. C. DeJONGHE, *J. Amer. Ceram. Soc.* **61** (1978) 185.

Received 22 April 1997
and accepted 30 July 1998